*Inorg. Chem.* **2007**, *46*, 3289–3294

# Study of the Insertion/Deinsertion Mechanism of Sodium into $Na_{0.44}MnO_2$

**F. Sauvage, L. Laffont, J.-M. Tarascon, and E. Baudrin***

*Laboratoire de Réactivité et Chimie des Solides, UMR CNRS 6007, Université de Picardie Jules Verne, 33 rue St. Leu, 80039 Amiens CEDEX France*

Received January 7, 2007

Pure $Na_{0.44}MnO_2$ samples were prepared via a solid-state route by carefully tuning the synthesis conditions. Insertion/deinsertion of sodium into the well-crystallized particles leads to capacities as high as 140 mA·h/g. A potentiostatic intermittent titration technic, together with in situ X-ray diffraction measurements, enabled us to evidence the presence of six biphasic transitions within a potential range of 2–3.8 V (vs $Na^+/Na$). The insertion process within the $Na_x$-$MnO_2$ system is fully reversible over the $0.25 < x < 0.65$ composition range and presents some degree of irreversibility as values of $x$ below 0.25 are reached. Furthermore, we similarly showed that HCl treatment has a detrimental effect on these electrochemical properties because of structural and textural evolutions.

## Introduction

While lithium-based battery technology is currently the premier energy storage system for portable applications, other alternative batteries based, for instance, on $Mg^{2+}$ [1] or $Na^+$ are far from being neglected. In the latter case, oxides,[2−5] phosphates,[6] and more recently fluorophosphates materials[7,8] were pointed out for their ability to reversibly accommodate sodium ions, enabling their use as a cathode for secondary battery applications. Among the small number of oxide materials of potential interest identified, $Na_{0.44}MnO_2$ is particularly attractive because of its adequate crystal structure forming suitable large-size tunnels for sodium incorporation.[9] However, in previous reports, the phases prepared by solid-state synthesis contained $Mn_2O_3$—bixbyite impurities. To avoid the presence of such parasitic phases, acidic treatment using HCl was used for their dissolution. However, this procedure concomitantly induces sodium leaching, leading to an isostructurally deficient sodium phase of approximate composition $Na_{0.20}MnO_2$.[9] Owing to the need for such an initial acid pretreatment, the intrinsic electrochemical properties of $Na_{0.44}MnO_2$ versus sodium have not been suitably exploited nor has the insertion mechanism been extensively examined. Recently, we pointed out the possibility of preparing pure $Na_{0.44}MnO_2$ powders by accurately adjusting the solid-state synthesis parameters and demonstrated further that this compound was also of great interest for sodium ion sensing applications.[10] On the basis of the fact that we can prepare pure $Na_{0.44}MnO_2$ directly, we enrolled in providing a detailed structural characterization by X-ray diffraction (XRD) and high-resolution transmission electron microscopy (HRTEM) and a complete electrochemical survey focused on the insertion/deinsertion mechanism of sodium in the $Na_{0.44}MnO_2$ structure. Finally, we will also stress the effect of the HCl pretreatment on the particle structure/texture and its consequences on the electrochemical behavior versus sodium.

## Experimental Section

Single-phase $Na_{0.44}MnO_2$ powders were obtained through a classic solid-state reaction using $MnCO_3$ and $Na_2CO_3$ (with a 10 wt % excess stoichiometry) intimately manually ground in a mortar.

* To whom correspondence should be addressed. E-mail: emmanuel.baudrin@u-picardie.fr. Tel.: +33-322827971. Fax: +33-322827590.

(1) Aurbach, D.; Lu, Z.; Schechter, A.; Gofer, Y.; Gizbar, H.; Turgeman, R.; Cohen, Y.; Moshkovitch, M.; Levi, E. *Nature* **2000**, *407*, 724−727.
(2) Tarascon, J.-M.; Hull, G. W. *Solid State Ionics* **1986**, *22*, 85−96.
(3) Braconnier, J. J.; Delmas, C.; Fouassier, C. *Mater. Res. Bull.* **1980**, *15*, 1797−1804.
(4) Shacklette, L. W.; Jow, T. R.; Townsend, L. *J. Electrochem. Soc.* **1988**, *135* (11), 2669−2674.
(5) Tarascon, J.-M.; Guyomard, D.; Wilkens, B.; McKinnon, W. R.; Barboux, P. *Solid State Ionics* **1992**, *57*, 113−120.
(6) Goodenough, J. B.; Hong, H. Y. P.; Kafalas, J. A. *Mater. Res. Bull.* **1976**, *11*, 203−220.
(7) Sauvage, F.; Quarez, E.; Tarascon, J.-M.; Baudrin, E. *Solid State Sci.* **2006**, *8*, 1215−1221.
(8) Barker, J.; Saidi, M. Y.; Swoyer, J. L. *J. Electrochem. Soc.* **2004**, *151* (10), A1670−A1677.
(9) Doeff, M. M.; Richardson, T. J.; Kepley, L. *J. Electrochem. Soc.* **1996**, *143* (8), 2507−2516.
(10) Sauvage, F.; Baudrin, E.; Tarascon, J. M. *Sens. Actuators, B* **2007**, *120*, 638−644.

10.1021/ic0700250 CCC: $37.00 
Published on Web 03/22/2007

To complete the reaction, this mixture was successively heated for 8 h at 300 °C and for 9 h at 800 °C under air with intermediate grindings. Following this procedure, a black powder was obtained. XRD patterns were collected in a $\theta-2\theta$ configuration using a Philips PW1729 with a Cu Kα anticathode ($\lambda = 0.15418$ nm). The particle morphology and the Na/Mn molar ratio were investigated by using an FEI Quanta 200 FEG environmental scanning electron microscope coupled with an energy-dispersive spectrometry (EDS) analysis system (Oxford Link Isis) and by atomic absorption spectroscopy (Perkin-Elmer model Analyst 300). For these latter experiments, 200 mg of powder was dissolved in concentrated sulfuric acid. The instrument was calibrated using four sets of known sodium and manganese concentrations. To further investigate the local structure of the pristine particles, HRTEM observations were carried out using a FEI TECNAI F20 S-TWIN microscope. The sample was first dispersed in ultrapure acetone before being deposited on a copper grid coated with a lacey-carbon film.

Electrochemical characterizations were made using the Bellcore plastic technology.[11] The active material was manually ground with 6 wt % of SP-type carbon black, 15 wt % of polyvinylidene difluoride−HFP copolymer, and 21 wt % of a dibutyl phthalate (DBP) plasticizer. Acetone was then added to the mixture to obtain a paste, which was subsequently cast over a glass plate. After drying, a plastic composite film was obtained and cut to the desired size. Prior to being used, the DBP plasticizer was extracted using diethyl ether (three washings of 10 min each). Open-circuit-voltage and Potentiostatic Intermittent Titration Technic (PITT) measurements were carried out in a two-electrode configuration in Swagelok-type cells assembled in an argon-filled glovebox and using metallic sodium as counter and reference electrodes. A Whatman GF/D borosilicate glass fiber sheet was used as the separator soaked with a 1 M $NaClO_4$/propylene carbonate (PC) electrolyte. The electrochemical tests were controlled by a VMP multipotentiostat (Biologic SA, Claix, France). In situ X-ray experiments were performed in a Scintag diffractometer using Cu Kα radiation with a homemade electrochemical cell formed with a beryllium window as a positive current collector. Because of the highly oxidative potential at the end of the charge, a thin protective aluminum layer was sputtered on this beryllium window. The electrochemical measurements were controlled by a Mac Pile system. The cell was cycled at a very low rate of ca. C/250 (reaction of one $Na^+$ in 250 h), and the interval between X-ray patterns corresponds to 0.006 inserted or deinserted $Na^+$. The lattice parameters refinements were performed using *Fullprof* software in the pattern-matching mode.

## Results and Discussion

**(a) Synthesis and Characterization of $Na_{0.44}MnO_2$.** Manganese oxides form a very rich and versatile structural family enlisting materials having either 1D-, 2D-, or 3D-type tunnel structures.[12] Among them, $Na_{0.44}MnO_2$, which is isostructural with $Na_4Mn_4Ti_5O_{18}$, crystallizes in an orthorhombic lattice cell (*Pbam* space group). The manganese ions are located in two different environments: all $Mn^{IV+}$ ions and half of the $Mn^{III+}$ ions are in octahedral sites ($MnO_6$), while the other $Mn^{III+}$ ions are gathered in a square-pyramidal environment ($MnO_5$). The latter forms edge-linked chains linked to two double and one triple octahedral chains by the vertices, leading to the formation of two types of tunnels. Two sodium sites (referenced as Na1 and Na2 in Figure 1) are situated in large S-shaped tunnels, while another site (Na3) is found in smaller tunnels.[13] According to this structure, the $\vec{c}$ direction is the main path for sodium diffusion. The entitled $Na_{0.44}$/Mn ratio corresponds to a filling of the Na3 sites, whereas the S-shaped tunnels are only half-filled.

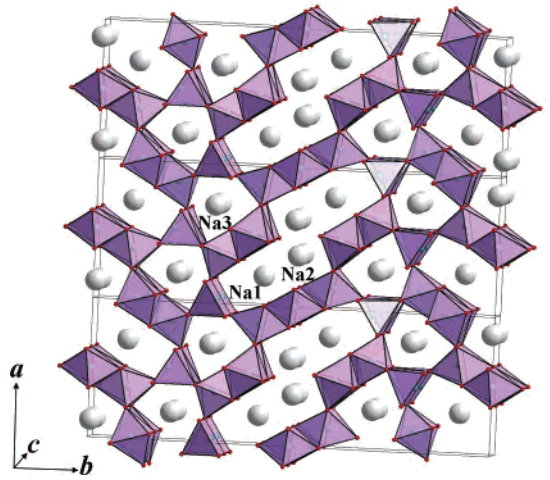


**Figure 1.** Representation of the structure of $Na_{0.44}MnO_2$ perpendicular to the *ab* plane.

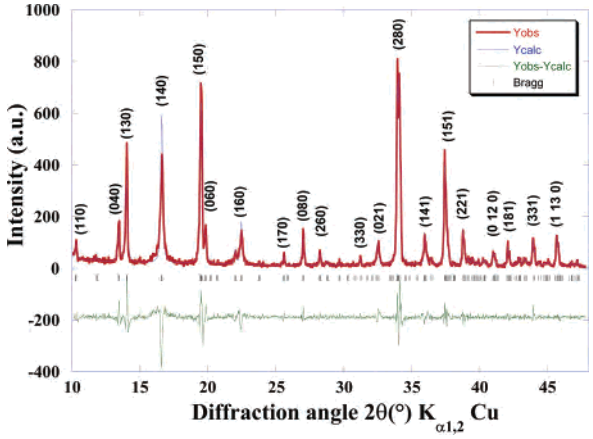


**Figure 2.** Results from the refinement of the XRD pattern of a $Na_{0.44}MnO_2$ powder in pattern-matching mode using *Fullprof*.

Following the synthesis conditions detailed to in the Experimental Section and previously reported by our group,[10] we obtained a well-crystallized $Na_{0.44}MnO_2$ powder without any visible traces of $Mn_2O_3$ impurities as underlined by the refined XRD pattern (Figure 2). The obtained lattice parameters are $a = 9.078(3)$ Å, $b = 26.44(1)$ Å, and $c = 2.827(1)$ Å, leading to a cell volume of 678 Å$^3$, in good agreement with previous reports.[9,10,14] The particles are well crystallized, as is observed with the presence of moiré (Figure 3), and have grown anisotropically, leading to rod shapes (length = 5−10 $\mu$m; width = 500 nm). The high-resolution picture exhibits an excellent atomic ordering arrangement with a

(11) Le Poul, N.; Baudrin, E.; Morcrette, M.; Gwizdala, S.; Masquelier, C.; Tarascon, J.-M. *Solid State Ionics* **2003**, *159*, 149−158.
(12) Thackeray, M. *Prog. Solid State Chem.* **1997**, *25*, 1−71.
(13) Doeff, M. M.; Ding, L.; De Jonghe, L. C. *Mater. Res. Soc. Symp. Proc.* **1995**, 393.
(14) Doeff, M. M.; Richardson, T. J.; Hollingsworth, J.; Yuan, C. W.; Gonzales, M. *J. Power Sources* **2002**, *112*, 294−297.

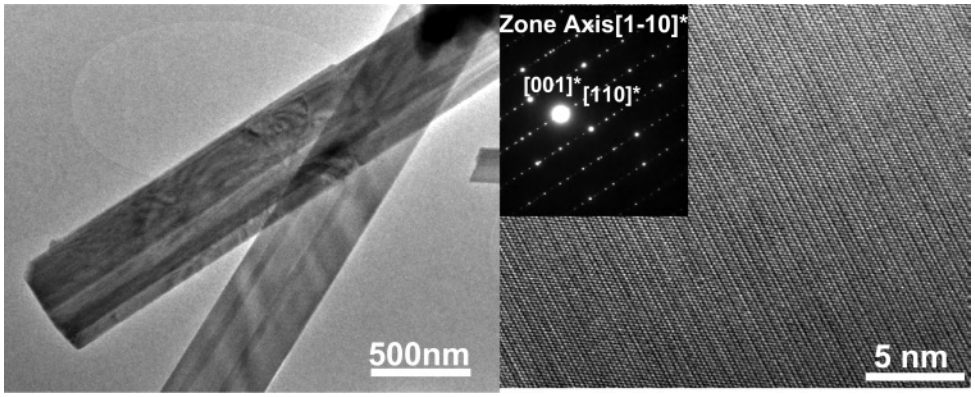


**Figure 3.** TEM and HRTEM images showing the rodlike $Na_{0.44}MnO_2$ particles synthesized by solid-state reaction and its structure [inset: selected area electron diffraction (SAED) pattern of this sample].

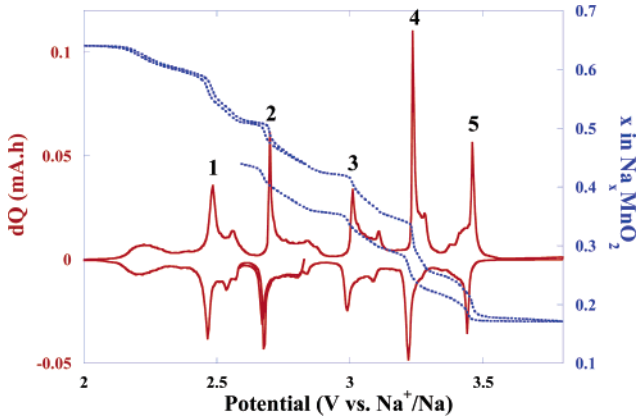


**Figure 4.** (blue dotted line) PITT curve starting at reduction (cycling rate of ca. C/200 with a 5 mV step) of the $Na_{0.44}MnO_2$/C composite electrode in an $NaClO_4$/PC electrolyte. (red solid line) Corresponding incremental capacity curve.

monolithic texture. Measurements realized by EDS (coupled with the HRTEM apparatus) and atomic absorption spectroscopy gave a homogeneous Na/Mn ratio with a value of 0.45 (±0.02), in good agreement with the expected compound.

**(b) Electrochemical Measurements of Composite $Na_{0.44}MnO_2$/C Electrodes.** To have a better insight into the electrochemical properties of $Na_{0.44}MnO_2$/C versus sodium, some very slow rate (i.e. C/200) PITT measurements were performed (corresponding to the reaction of one $Na^+$ ion in 200 h). Within the potential range 2−3.8 V (vs $Na^+$/Na), several phenomena are observed, with the composition varying between $x = 0.18$ and 0.64 in $Na_xMnO_2$ (Figure 4). Such a potential−composition ($E$ vs $x$) curve obviously underlines the complexity of the insertion/deinsertion mechanism and looks very similar to the one reported by Doeff et al.[9] It is amazing to notice that, in general, the insertion of sodium ions leads to such multitransition processes as those illustrated by other oxides such as, for instance, the $Na_xCoO_2$ compound.[3,4] Over the voltage range 3.8−2 V, a specific capacity of about 140 mA·h/g is reached, one of the highest capacities reported to date among the $Na^+$ insertion materials.[2−8,15] We can also appreciate the very low polarization obtained when the cell is launched directly in reduction. Nevertheless, when the samples are fully oxidized to 3.8 V and then reduced, we observe a large shift in the onset values of the various features on the voltage/composition trace, indicative of an irreversible capacity phenomenon when the samples get through the two highest-voltage plateaus. Bearing in mind the above-described structure, such a finding regarding the degree of reversibility of the observed capacities means that the Na1 and Na2 sites located in the S-type tunnels are reversibly accessible (composition of $0.22 < x < 0.66$) while the sodium ions located on the Na3 site are not or hardly extracted.

The incremental capacity curve (Figure 4) obtained in PITT mode is consistent with the presence of at least five biphasic transitions on narrow domains within this composition range. Indeed, while from the current decreases it is difficult to clearly identify the phenomena (not shown here), the obtained sharp peaks are characteristic of such two-phase transitions and the smaller and broader ones are reminiscent of single-phase evolution, as we will underline in the following. Furthermore, during our investigation of this material in an aqueous electrolyte [$NaNO_3$ (1 M)/$H_2O$], we also clearly evidenced the existence of another transition occurring close to the $Na_{0.44}MnO_2$ composition.[10] However, at this point, the presence of such a transition is less obvious using the nonaqueous $NaClO_4$ (1 M)/PC electrolyte. Interestingly, we can notice that five independent manganese sites are found in this structure. However, at the present time, it is difficult to clearly and simply make a correlation with the observed transitions.

**(c) In Situ XRD Measurements during the Insertion/Deinsertion of Sodium.** To clearly evaluate the structural evolution of the entitled material during the insertion/deinsertion process, we undertook some in situ XRD measurements using specific cells comprising a beryllium window as the current collector. Owing to the complex mechanism underlined by the PITT electrochemical curve and the quite narrow composition domains of the different phases involved, we carried out these measurements at a low rate of ca. C/250. In spite of the numerous diffractograms hereby recorded as the $Na_{0.44}MnO_2$ phase was either electrochemically oxidized (Figure 5a) or reduced (Figure 5b), it is difficult to clearly distinguish the appearance of a new

(15) Morales, J.; Santos, J.; Tirado, J. L. *Solid State Ionics* **1996**, *83*, 57−64.

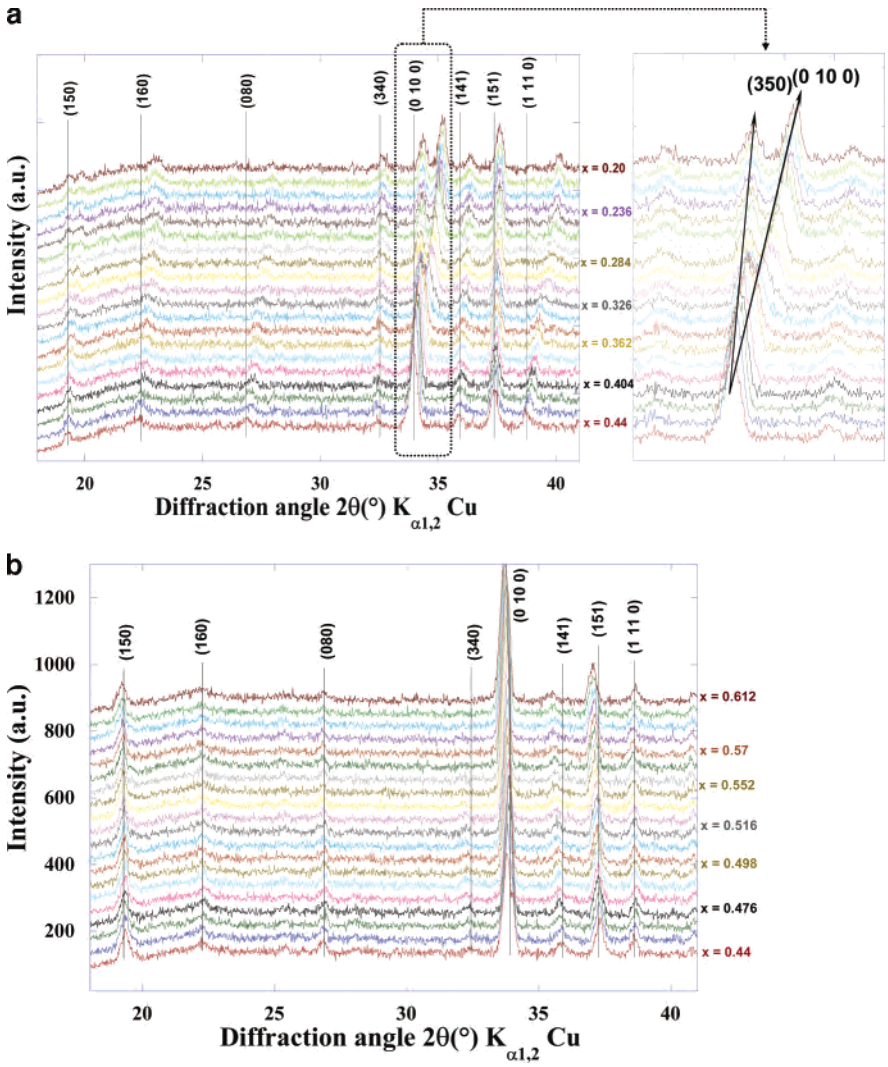


**Figure 5.** In situ evolution of the XRD pattern recorded at a C/250 charge/discharge rate: (a) upon reduction; (b) upon oxidation of $Na_{0.44}MnO_2$.

phase at the expense of another. However, because of the evolution of the cell parameters, we detect clear shifts of a few diffraction lines such as, for instance, the splitting of the (350) reflection into Bragg peaks assigned as (350) and (0 10 0) (Figure 5a). As a result of the evolution of the XRD patterns and in relation to the electrochemical curve, we can expect that the phases, which would be formed during biphasic transitions upon insertion/deinsertion into $Na_{0.44}MnO_2$, are structurally very close. The possibility of sodium ordering within the structure, which could be responsible for different biphasic transitions, can be ruled out because no superstructures have been evidenced by either HRTEM or XRD. All of the diffractograms recorded during the in situ investigations have been refined using the *Fullprof* software.[16] From the evolution of the cell parameters as a function of the sodium composition (Figure 6), we can clearly distinguish biphasic transition domains in agreement with the PITT measurements (reported as gray domains). Furthermore, at a composition close to $x = 0.44$, there is also a parameter jump characteristic of such a transition and coherent with our previous measurements in aqueous media.[10] All of these evolutions again underline that the electrochemical insertion/deinsertion within the studied composition range does not proceed through a single solid solution mechanism but through several multiphase reactions. Between successive transitions, Vegard's law is usually verified (Figure 6). Finally, it is worthwhile to notice that the sodium deinsertion process from $Na_{0.44}MnO_2$ affects mainly the *b* parameter and only slightly the *a* and *c* parameters while the opposite (slight variation of *b* and a strong variation of *a* and *c*) occurs when sodium ions are electrochemically inserted into $Na_{0.44}MnO_2$. However, at this state of the study, it is difficult to link this evolution to the site occupancy of sodium in the different sites.

**(d) $Na_{0.44}MnO_2$/C Composite Electrode Behavior upon Cycling.** The cycling life of the $Na_{0.44}MnO_2$/C electrode has been investigated in a galvanostatic mode at a C/10 rate (Figure 7). The capacity retention is not good because only about half of the capacity is retained after 50 cycles. As depicted by the inset, while conserving the different electrochemical phenomena, this capacity loss is associated with a noticeable cell polarization increase probably nested in the

(16) *Fullprof* (version Dec 2005); Roisnel (LCSIM, Rennes), J.; Rodriguez-Carjaval, L. L. B. (CEA-CNRS), France, 2005.

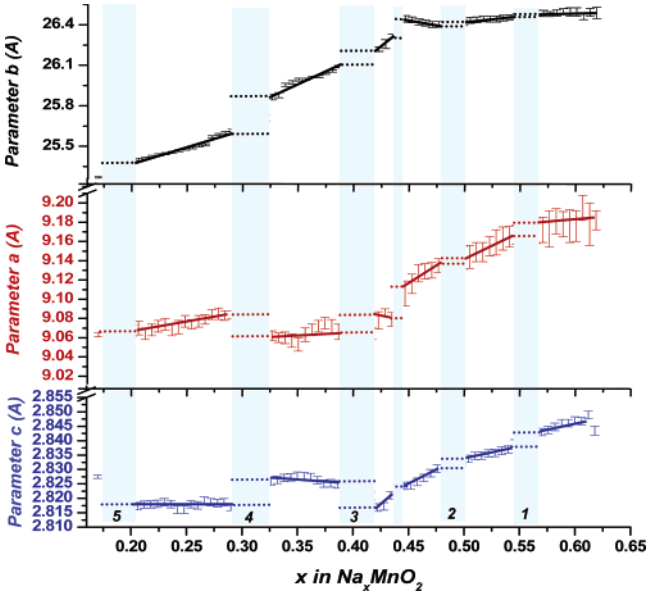


**Figure 6.** Evolution of *a*, *b*, and *c* parameters as a function of the sodium composition in $Na_xMnO_2$.

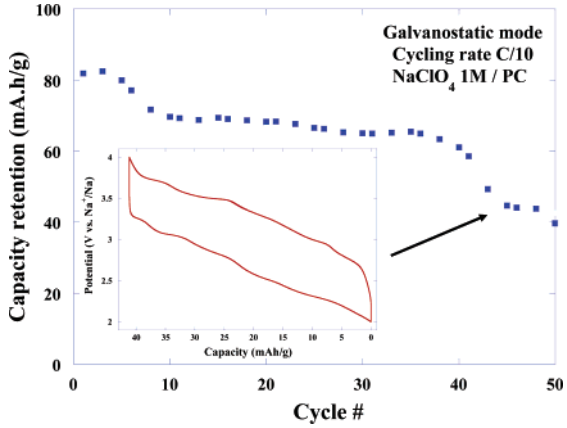


**Figure 7.** Capacity retention upon cycling of a $Na_{0.44}MnO_2$/C composite electrode at a C/10 rate (inset: illustration of the electrochemical curve recorded after 45 cycles).

succession of electrochemical oxidation. At this point, we cannot rule out the possible influence of the sodium anode on this capacity loss. Indeed, in a typical electrolyte, there is no proper passivation of sodium as known for lithium. This is also consistent with previous works showing that the capacity retention is good in lithium cells with preservation of the structure after deintercalation.[17] Similarly, as soon as the electrode is cycled faster than C/20, a drastic decrease in the capacity is noticed, thus demonstrating some kinetic limitations. Besides the irreversible phenomenon described at high voltage (Figure 4), we also observed a self-discharged phenomenon for two distinct electrolytes [$NaClO_4$ (1 M)/PC and 1:1 NaTFSI (1 M) EC/DMC]. This process, which is faster in $NaClO_4$ (1 M)/PC, leads to an X-ray amorphous phase and could also be partly at the origin of the observed loss capacity upon cycling. However, thorough experiments are needed to better understand the self-discharge mechanism.

**(e) Structural and Electrochemical Effects of the Acidic HCl Pretreatment.** As mentioned earlier, some $Mn_2O_3$ impurities are classically concomitantly formed with $Na_{0.44}MnO_2$ when the synthesis conditions are not efficiently tuned. To bypass the formation of this impurity, HCl pretreatment was used to dissolve such $Mn_2O_3$. However, such a pretreatment is not neutral for the $Na_{0.44}MnO_2$ phase because its composition evolved to a sodium-deficient composition of ca. $Na_{0.20}MnO_2$.[8] We performed in this work an acidic pretreatment (using 0.1 M HCl for 24 h) to clearly evaluate its effect on the texture and electrochemical properties. While the rodlike morphology is preserved, an EDS analysis leads to the $Na_{0.17}MnO_2$ composition. A similar composition is typically obtained when using a stronger oxidant reagent like $NO_2BF_4$. HRTEM images evidence, however, some fractures and underline crystallographic defaults of 10 nm depth within the particles (Figure 8). Furthermore, such an acidic treatment induces an evolution of the cell parameters [$a$ = 9.063(2) Å, $b$ = 25.269(5) Å, and $c$ = 2.8275(5) Å]. The latter are consistent with the cell evolution during the electrochemical oxidation (Figure 6), the Na/Mn = 0.17 ratio, and the parameters obtained by Doeff et al.[8] for their synthesized powders. Although the different insertion/deinsertion phenomena were clearly visible on the electrochemical signature in the pristine compound, the HCl-treated material shows a smoother voltage evolution and an increased polarization (~500 vs ~70 mV for $Na_{0.44}MnO_2$ cycled under the same conditions; Figure 9). The lattice cell contraction of around 4.5%, together with the crystallographic defects surrounding the particles, can be at the origin of the increased kinetic limitations. These limitations, formed when the material is highly oxidized, are also consistent with the potentiometric measurements reported in ref 10 (e.g., a longer response time at the oxidized state).

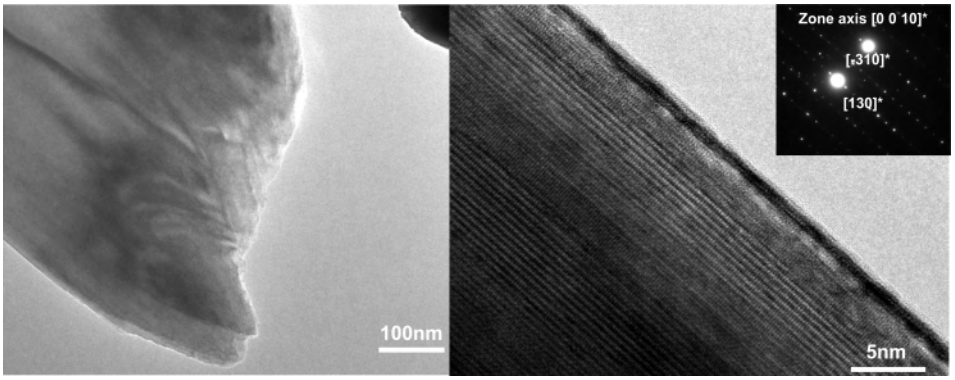


**Figure 8.** TEM and HRTEM images of $Na_{0.17}MnO_2$ particles (obtained by HCl treatment of $Na_{0.44}MnO_2$) and the related SAED pattern.

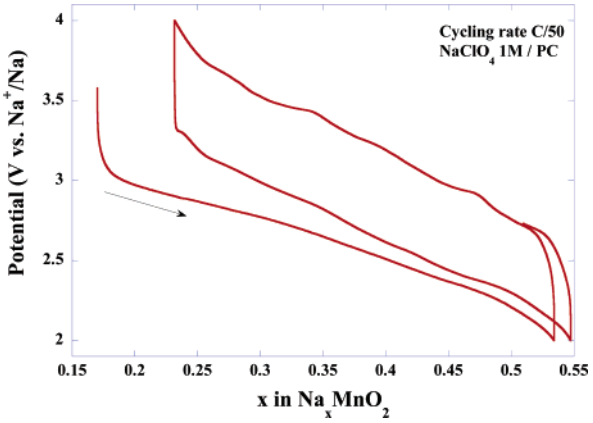


**Figure 9.** Galvanostatic curve of a $Na_{0.17}MnO_2$/C composite electrode at a cycling rate of C/50 in $NaClO_4$ (1 M)/PC.

Again, it underlined the importance of directly obtaining the $Na_{0.44}MnO_2$ phase if we want to evaluate the intrinsic electrochemical properties. Indeed, the acidic treatment on such a phase induces an oxidation resulting from a disproportion/dissolution phenomenon, typically encountered for $Mn^{III+}$-containing phases, and which is detrimental to good lithium diffusion. However, keeping in mind also the irreversible electrochemical phenomenon at high voltage (Figure 5), we cannot rule out the possibility of oxygen nonstoichiometry or the creation of other defects[18] when this phase is highly oxidized either chemically or electrochemically. This is also consistent with the evolution of the texture noticed by HRTEM and the increase of polarization. Such an influence of nonstoichiometry on the electrochemical properties was previously reported for several sodium insertion materials such as $Na_xCoO_2$[3] and $Na_xMo_2O_4$.[2] Further experiments will be needed to clarify this point.

## Conclusion

In this work, by carefully controlling the synthesis conditions, we were able to obtain the single phase $Na_{0.44}MnO_2$. The direct formation of this phase is important because the acidic treatment generally used to eliminate impurities has a drastic effect on the electrochemical properties of such manganese oxides. We clearly evidenced the complexity of the sodium insertion/deinsertion process with at last six distinct biphasic phenomena between 2 and 3.8 V (vs $Na^+/Na$) within a $0.18 < x < 0.64$ composition range (in $Na_xMnO_2$). However, it appears that the different phases are close and related to the structure of $Na_{0.44}MnO_2$. When the latter is highly oxidized, the sodium insertion/deinsertion process exhibits a noticeable polarization increase and a capacity decrease. Further work is needed to limit the self-discharge effect either by coating of the particles or via substitution similar to the approach followed for the spinel $LiMn_2O_4$.[19]

**Acknowledgment.** The authors thank Sylvain Topin for his valuable experimental help on this survey.

IC0700250

(17) Doeff, M. M.; Anapolsky, A.; Edman, L.; Richardson, T. J.; de Jonghe, L. C. *Electrochem. Soc.* **2001**, *148*, A230.
(18) Floros, N.; Michel, C.; Hervieu, M.; Raveau, B. *J. Solid State Chem.* **2001**, *162*, 34−41.
(19) Amatucci, G. G.; Pereira, N.; Zheng, T.; Tarascon, J.-M. *J. Electrochem. Soc.* **2001**, *148* (2), A171−A182.